Superfocusing of channeled protons and subatomic measurement resolution

S. Petrović,* N. Nešković, V. Berec, and M. Ćosić
Laboratory of Physics, Vinča Institute of Nuclear Sciences, University of Belgrade, P.O. Box 522, 11001 Belgrade, Serbia
(Received 8 December 2011; published 7 March 2012)

In this work we analyze the superfocusing of protons channeled in a ⟨100⟩ Si thin crystal using the theory of crystal rainbows. The initial proton energy is 68 MeV and the proton beam incident angle is increased gradually from zero up to 30% of the critical angle for proton channeling. The reduced crystal thickness is varied around 0.250, the corresponding crystal thickness being 481.8 nm. The spatial distributions of channeled protons, obtained by the numerical solution of the proton equations of motion in the transverse position plane and a Monte Carlo computer simulation code, are explored as functions of the beam incident angle and reduced crystal thickness. They are analyzed via the corresponding mappings of the impact parameter plane to the transverse position plane, which are characterized by the rainbow effect. The performed analysis shows that it is possible to focus the beam within the region of the radius considerably below the Bohr radius. The obtained results provide the theoretical basis for the possible development of a measurement technique with the picometer resolution—the rainbow subatomic microscopy.

DOI: 10.1103/PhysRevA.85.032901 PACS number(s): 61.85.+p

I. INTRODUCTION

In recent years, as the characteristic dimensions of devices made of advanced materials have approached the nanometer scale, obtaining the information on the relationship between their structure and properties around this limit has emerged as a fundamental request in materials and devices engineering [1,2]. On the other hand, one of the major driving forces in the field of ion channeling in crystals is the requirement to guide and focus ion beams to nanometer sized regions [3,4]. Our study is connected to this requirement.

It was found in the early days of studying ion channeling that when the statistical equilibrium in the transverse phase space is established, the yield of ions is maximal on the channel axis. However, in the initial stage of propagation of the ion beam through the channel, the yield of ions on the channel axis oscillates about the line close to the one corresponding to the statistical equilibrium. That effect was named the flux peaking effect in ion channeling [5–18]. The leading idea in all those studies was to measure the yield of ions that were backscattered within the channels in order to determine the locations of foreign atoms in the crystal.

Demkov and Meyer [19] reopened the theoretical studying of the flux peaking effect before establishing the statistical equilibrium in the transverse phase space, but with the idea to apply it for subatomic microscopy. Since the effect was qualitatively different from the flux peaking effect after establishing the statistical equilibrium, they named it differently—the superfocusing effect in ion channeling. Following the theoretical studies of Miletić *et al.* [20,21], those authors analyzed the spatial focusing of protons of the initial energy of 1 MeV in the ⟨100⟩ channel of a Si thin crystal assuming that the continuum proton-crystal interaction potential was dominantly cylindrically symmetric and harmonic. The superfocusing effect was also considered by us [22]. We treated it as the crystal rainbow effect [23,24], whose occurrence had been confirmed experimentally by Krause *et al.* [25,26]. In that analysis we used the theory of crystal rainbows, which had been formulated by Petrović *et al.* [27] as the proper theory of ion channeling in thin crystals. We investigated the superfocusing of 2 MeV protons channeled along the ⟨100⟩ axis of a Si thin crystal in the vicinity of the superfocusing point in the first rainbow cycle, i.e., for the reduced crystal thickness around 0.250. The reduced crystal thickness is defined as $\Lambda = f_h L/v_0$, where L is the crystal thickness, v_0 the initial proton velocity, and f_h the frequency of proton motion close to the channel axis. The continuum proton-crystal interaction potential was of the Thomas-Fermi type, having both the harmonic and anharmonic components. We did not take into account the effects of collisions of the proton and the crystal's electrons.

This study is the continuation of the work of Demkov and Meyer [19] and of our previous study [22]. We shall report on the superfocusing of 68 MeV protons channeled in the ⟨100⟩ Si thin crystal in the vicinity of the superfocusing point in the first rainbow cycle for different values of proton beam incident angle. Our aim is to demonstrate that it is possible to use such a beam, whose half-width can be made much smaller than the Bohr radius, to probe a foreign atom inserted in the channel in the vicinity of the superfocusing point. The scanning of the interior of the foreign atom is performed by changing the beam incident angle. This means that the superfocused beam could help us achieve the picometer measurement resolution. This approach has the potential for a breakthrough in the field of subatomic microscopy. In order to outline the main features of the superfocusing effect, we shall analyze the spatial distributions of channeled protons, i.e., their distributions in the transverse position plane, for different values of beam incident angle and reduced crystal thickness. That will be done with the effects of collisions of the proton and the crystal's electrons taken into account. We shall also explore the rainbow patterns corresponding to these distributions.

II. THEORY

The system to be analyzed here is a proton moving through the ⟨100⟩ channel of a Si thin crystal. The interaction of the

*petrovs@vinca.rs

proton and a crystal's atom is described by the Thomas-Fermi interaction potential in Molière's approximation [28–30], which reads

$$V(r') = \frac{Z_1 Z_2 e^2}{r'}[0.35\exp(-br') + 0.55\exp(-4br') + 0.10\exp(-20br')], \quad (1)$$

where Z_1 and Z_2 are the atomic numbers of the hydrogen and silicon atoms, respectively, e is the elementary charge, r' is the distance between the proton and the crystal's atom, $b = 0.3/a$, $a = [9\pi^2/(128Z_2)]^{1/3}a_0$ is the screening radius of the atom, and a_0 is the Bohr radius. The z axis of the reference frame is taken to coincide with the $\langle 100\rangle$ axis with the origin lying in the entrance plane of the crystal. The x and y axes of the reference frame are the vertical and horizontal axes, respectively. The proton beam axis lies in the xz plane and makes angle φ with the z axis, being the beam incident angle. We further apply the continuum approximation [28]. As a result, the continuum interaction potential of the proton and crystal is obtained as a sum of the continuum interaction potentials of the proton and the crystal's atomic strings,

$$U^{\rm th}(x,y) = \sum_{i=1}^{M} U_i^{\rm th}(x,y), \quad (2)$$

where x and y are the transverse components of the proton position and M is the number of atomic strings. This expression includes the thermal vibrations of the atoms. The continuum interaction potential of the proton and ith atomic string is

$$U_i^{\rm th}(x,y) = U_i(x,y) + \frac{\sigma_{\rm th}^2}{2}[\partial_{xx}U_i(x,y) + \partial_{yy}U_i(x,y)], \quad (3)$$

where $U_i(x,y)$ is the continuum interaction potential of the proton and ith atomic string without the effect of thermal vibrations taken into account, obtained using Eq. (1), and $\sigma_{\rm th}$ the one-dimensional thermal vibration amplitude of the atoms [29].

Unlike in our previous study [22], we include in the calculations of the spatial distributions of channeled protons the effects of their collisions with the crystal's electrons. The specific (electronic) energy loss of the proton in the channel is taken into account via relation

$$-\frac{dE}{dz} = \frac{4\pi Z_1^2 e^4}{m_e v^2} n_e \ln\frac{2m_e v^2}{\hbar\omega_e}, \quad (4)$$

where m_e is the electron mass, v the proton velocity, $n_e = \triangle U^{\rm th}(x,y)/(4\pi)$ the density of the crystal's electron gas averaged along the z axis, $\triangle = \partial^2/\partial x^2 + \partial^2/\partial y^2$, $\hbar$ the reduced Planck constant, and $\omega_e = (4\pi e^2 n_e/m_e)^{1/2}$ the angular frequency of the electron gas oscillations induced by the proton [29,31]. The specific change of the dispersion of the proton channeling angle caused by its collisions with the electrons is included in the form

$$\frac{d\Omega^2}{dz} = \frac{m_e}{m_p^2 v^2}\left(-\frac{dE}{dz}\right), \quad (5)$$

where m_p is the proton mass [29,32]. The corresponding dispersions of the components of the proton channeling angle are $\Omega_x^2 = \Omega_y^2 = \Omega^2/2$.

Our calculations are based on the theory of crystal rainbows. They are concentrated on the appearance of rainbows in the proton transmission through the $\langle 100\rangle$ channel of a Si thin crystal when the proton beam axis does not coincide with the channel axis, i.e., when the crystal is tilted relative to the plane perpendicular to the beam axis. This theory enables us to analyze the spatial distributions of channeled protons via the corresponding rainbow patterns. These distributions are generated using the numerical solution of the proton equations of motion in the transverse position plane and a Monte Carlo computer simulation code.

The analysis of the proton transmission process in question is carried out via the mapping of the impact parameter plane to the transverse position plane [22,23,33,34] for the chosen values of φ and reduced crystal thickness Λ. The Jacobian of this mapping, i.e., the ratio of the infinitesimal surfaces in the transverse position plane and impact parameter plane, reads

$$J_\rho(x_0,y_0,\varphi,\Lambda) = \frac{\partial x}{\partial x_0}\frac{\partial y}{\partial y_0} - \frac{\partial x}{\partial y_0}\frac{\partial y}{\partial x_0}, \quad (6)$$

where x_0 and y_0 are the components of the proton impact parameter, i.e., the transverse components of its initial position. Thus, equation $J_\rho(x_0,y_0,\varphi,\Lambda) = 0$ determines the lines in the impact parameter plane along which the proton yield in the transverse position plane is singular. We analyze here the images of these lines in the transverse position plane, i.e., the rainbow lines in this plane. In order not to make these calculations too complex, we do not include in them the effects of collisions of the proton and the crystal's electrons. However, as has been said above, these effects are taken into account in the calculations of the spatial distributions of channeled protons.

III. RESULTS AND DISCUSSION

Let us now concentrate on the superfocusing of protons channeled in the $\langle 100\rangle$ Si thin crystal for various values of proton beam incident angle φ. The initial proton energy E_0 is 68 MeV and the reduced crystal thickness Λ is changed within the first rainbow cycle. We shall explain the choice of the value of E_0 later. The values of φ are chosen between 0 and $\pm 0.30\psi_c$, where $\psi_c = [2Z_1Z_2e^2/(dE_0)]^{1/2} = 1.04$ mrad is the critical angle for proton channeling, with d being the distance between the crystal's atoms within the atomic strings [28]. The one-dimensional thermal vibration amplitude of the atoms is $\sigma_{\rm th} = 7.4$ pm [35]. We assume that the crystal's atomic strings defining the channel intersect the x and y axes. The number of atomic strings is 36; i.e., we take into account the atomic strings lying on the three nearest square coordination lines [27]. The proton equations of motion in the transverse position plane are solved numerically using the Runge-Kutta method of the fourth order [36]. The components of the proton impact parameter, x_0 and y_0, are chosen randomly from the uniform distributions within the region of the channel. The initial proton velocity vectors are all parallel to the beam axis. The initial number of protons is 4 352 720.

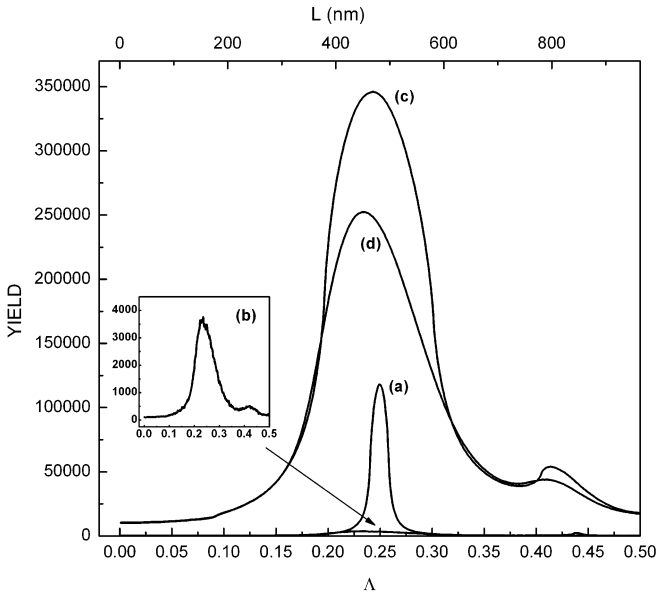

FIG. 1. The yields of channeled protons in the region of the transverse position plane around the origin in which r is smaller than $a_1 = 0.5$ pm without and with the effects of the crystal's electrons taken into account—dependencies (a) and (b), respectively—and in the region around the origin in which r is smaller than $a_1 = 0.75$ pm without and with the effects of the crystal's electrons taken into account—dependencies (c) and (d), respectively—as functions of the reduced crystal thickness Λ or the crystal thickness L in the first rainbow cycle for the proton beam incident angle $\varphi = 0$.

A. Spatial distributions

Figure 1 shows the yield of channeled protons around the origin in the transverse position plane as a function of Λ or L, i.e., their axial yield, without taking into account the effects of collisions of the proton and the crystal's electrons. For the region in the transverse position plane around the origin we take the region in which the radial component of the proton position, $r = (x^2 + y^2)^{1/2}$, is smaller than $a_1 = 0.01a_0 = 0.5$ pm, where $a_0 = 52.9$ pm is the Bohr radius. This dependence contains one maximum at $\Lambda_m = 0.250$, corresponding to $L_m = 481.8$ nm, being the superfocusing point in the first rainbow cycle. Hence, one concludes that this maximum occurs due to the superfocusing of channeled protons, which is explained by the dominance of the harmonic component of the continuum proton-crystal interaction potential, given by Eq. (2), over its anharmonic component in the region close to the channel axis [19,22]. Its width, being a measure of the longitudinal extent of the superfocusing region, is $\Delta\Lambda_f = 0.018$ or $\Delta L_f = 34.7$ nm. The figure also gives the axial yield of channeled protons for $a_1 = 0.5$ pm with the effects of the crystal's electrons taken into account. Now, the superfocusing maximum is much weaker and broader than the corresponding maximum obtained without taking into account the effects of the crystal's electrons. It is located at $\Lambda_m = 0.235$, corresponding to $L_m = 452.9$ nm, and its width is $\Delta\Lambda_f = 0.088$ or $\Delta L_f = 169.6$ nm. The weakening and broadening of the superfocusing maximum is attributed to the spreading of the spatial distribution of channeled protons caused by the effects of the crystal's electrons. Its shift from the superfocusing point, being $\Delta\Lambda_m = 0.015$ or $\Delta L_m = 28.9$ nm, can be explained if the evolution of the rainbow line in the transverse position plane in the vicinity of the superfocusing point described in Ref. [22] is taken into account. It is caused by the difference between the evolution of the rainbow line after the superfocusing point, for Λ above 0.250, and the time-reversed evolution of the rainbow line before the superfocusing point, for Λ below 0.250. Namely, in the former case, the rainbow line moves away from the origin faster than in the latter case, resulting in a decrease of the axial proton yield in the former case and an increase of the yield in the latter case. This difference becomes observable due to the spreading of the spatial distribution. It is evident that the increase of $\Delta\Lambda_f$ or ΔL_f when one takes into account the effects of the crystal's electrons is not negligible. If E_0 were chosen to be 2 MeV, as it was the case in Ref. [22], this increase would be even more pronounced. The analysis showed that in that study the effects of the crystal's electrons were underestimated. Being aware of that and in order to minimize the effects of the crystal's electrons, we chose for E_0 the above specified value of 68 MeV, appearing in a series of relevant experiments [37,38].

Besides, Fig. 1 gives the axial yield of channeled protons for $a_1 = 7.5$ pm without taking into account the influence of the crystal's electrons. The choice of this value of a_1 will be explained later. In this case, the superfocusing maximum is located at $\Lambda_m = 0.243$, corresponding to $L_m = 468.3$ nm, and its width is $\Delta\Lambda_f = 0.105$ or $\Delta L_f = 202.4$ nm. The small shift of the superfocusing maximum from the superfocusing point, being $\Delta\Lambda_m = 0.002$ or $\Delta L_m = 3.9$ nm, is explained by the difference between the evolution of the rainbow line after the superfocusing point and the time-reversed evolution of the rainbow line before the superfocusing point, which becomes observable due to the larger value of a_1. The figure also shows the axial yield of channeled protons for $a_1 = 7.5$ pm with the influence of the crystal's electrons taken into account. In this case, the superfocusing maximum is weaker and broader than the corresponding maximum obtained without taking into account the influence of the crystal's electrons. It is located at $\Lambda_m = 0.234$, corresponding to $L_m = 451.0$ nm, and its width is $\Delta\Lambda_f = 0.114$ or $\Delta L_f = 219.7$ nm. The weakening and broadening of the superfocusing maximum are attributed to the spreading of the spatial distribution of channeled protons caused by the influence of the crystal's electrons. Its additional shift from the superfocusing point, being $\Delta\Lambda_m = 0.016$ and $\Delta L_m = 30.8$ nm, is attributed to the difference between the evolution of the rainbow line after the superfocusing point and the time-reversed evolution of the rainbow line before the superfocusing point, which becomes more observable due to the spreading of the spatial distribution.

Figure 2(a) gives the spatial distributions of channeled protons along the x axis for seven values of the proton beam incident angle, $\varphi = 0$, $\pm 0.10\psi_c$, $\pm 0.20\psi_c$, and $\pm 0.30\psi_c$, and $\Lambda = 0.250$ with the effects of collisions of the proton and the crystal's electrons taken into account. Each of these distributions contains one maximum, appearing due to the superfocusing effect. The width of the maximum for $\varphi = 0$, lying at the origin, is $\Delta x_m = 15$ pm. This width represents the beam diameter for $\varphi = 0$ and $\Lambda = 0.250$. The calculations showed that for Λ above 0.250, Δx_m increased abruptly, that for Λ between 0.250 and 0.225, it practically stayed the same, and that for Λ below 0.225, it increased abruptly too. This

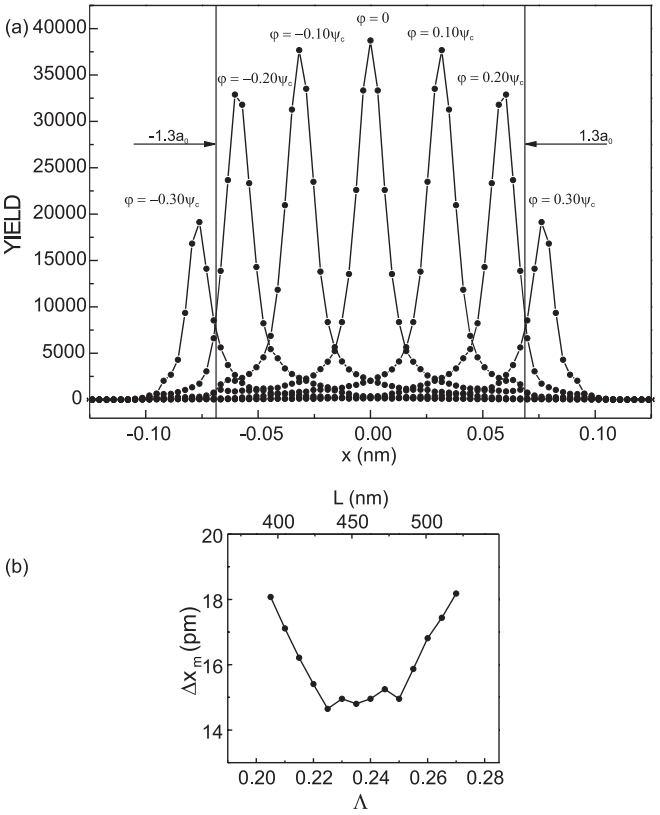

FIG. 2. (a) The yields of channeled protons along the x axis in the transverse position plane for the proton beam incident angles $\varphi = 0$, $\pm 0.10\psi_c$, $\pm 0.20\psi_c$, and $\pm 0.30\psi_c$ and the reduced crystal thickness $\Lambda = 0.250$, corresponding to the crystal thickness $L = 481.8$ nm, with the effects of the crystal's electrons taken into account. (b) The width of the spatial distribution of channeled protons along the x axis in the transverse position plane, Δx_m, as a function of the reduced crystal thickness, Λ, or the crystal thickness, L, in the vicinity of the superfocusing point in the first rainbow cycle for the proton beam incident angle $\varphi = 0$ with the effects of the crystal's electrons taken into account.

is illustrated in Fig. 2(b). Thus, one can call the part of the superfocusing region between $\Lambda = 0.225$ and 0.250 the beam neck. Its length is $\Delta\Lambda_n = 0.025$ or $\Delta L_n = 48.2$ nm. Accordingly, we decided to adopt that within the beam neck the value of its diameter was equal to its value for $\Lambda = 0.250$ (15 pm). That was the reason for choosing the larger value of a_1 (7.5 pm) in the analysis of the axial yield of channeled protons, whose results are given in Fig. 1.

As one would expect, for the positive values of φ, the maxima of the spatial distributions of channeled protons given in Fig. 2(a) lie on the positive part of the x axis, and for the negative values of φ, on the negative part of the x axis. The larger the modulus of φ, the larger the displacement of the maximum from the origin. Also, when the modulus of φ is larger, the maximum is weaker. The positions of the maxima for $\varphi = \pm 0.10\psi_c$, $\pm 0.20\psi_c$, and $\pm 0.30\psi_c$ are ± 31.8 pm, ± 60.3 pm, and ± 76.2 pm, respectively, while their heights are 97.3, 84.9, and 49.4 % of the height of maximum for $\varphi = 0$, respectively. Therefore, one can say that the maxima for $\pm 0.10\psi_c$ and $\pm 0.20\psi_c$, whose displacements from the origin are below $1.3a_0$ and above $-1.3a_0$, respectively, are strong, as the maximum for $\varphi = 0$. On the other hand, the maxima for $\varphi = \pm 0.30\psi_c$, whose displacements from the origin are above $1.3a_0$ and below $-1.3a_0$, respectively, are weak. This suggests that by varying φ from 0 to $\pm 0.20\psi_c$, one can probe the interior of a foreign atom inserted in the channel at a depth around $\Lambda = 0.250$, i.e., in the vicinity of the superfocusing point [22]. The weakening of the superfocusing effect for $\varphi = \pm 0.30\psi_c$ can be attributed to the fact that in this case the proton beam is displaced considerably from the channel axis toward the upper or lower channel wall, respectively, and moves through the region of the channel in which the anharmonic component of the interaction potential and the effects of the crystal's electrons are more pronounced than in the region close to the channel axis [22]. It should be noted that the spatial distributions given in the figure were calculated for $\Lambda = 0.250$ in spite of the fact that the maximum of dependence (d) shown in Fig. 1 lay at $\Lambda_m = 0.234$. The reasons for such a choice were the facts that the shift of that maximum from the superfocusing point, being $\Delta\Lambda_m = 0.016$, was within the beam neck, extending between $\Lambda = 0.225$ and 0.250, and that point $\Lambda = 0.250$ is the superfocusing point.

The spatial distributions of channeled protons in the two-dimensional representation for $\varphi = 0, \pm 0.10\psi_c, \pm 0.20\psi_c$, and $\pm 0.30\psi_c$ and $\Lambda = 0.250$ are shown in Fig. 3. It is evident that each of the distributions has one maximum. The shapes of the areas of the distributions for $\varphi = 0$ and $\pm 0.10\psi_c$ representing

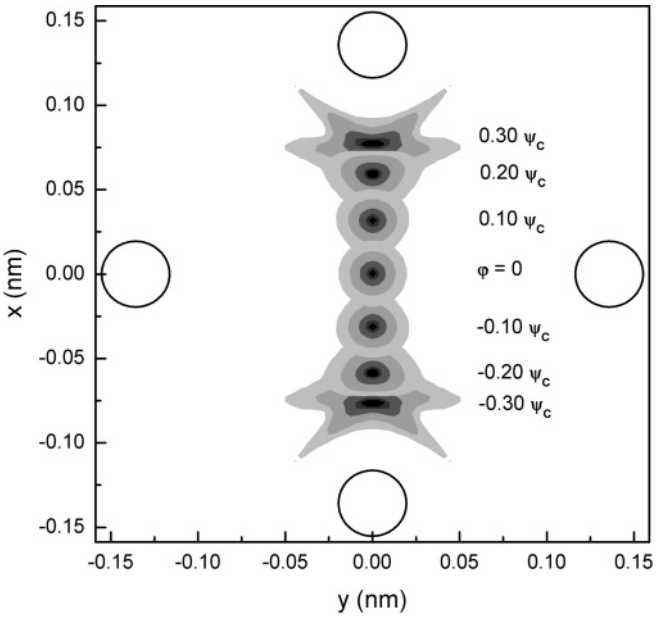

FIG. 3. The yields of channeled protons in the transverse position plane in the two-dimensional representation for the proton beam incident angles $\varphi = 0$, $\pm 0.10\psi_c$, $\pm 0.20\psi_c$, and $\pm 0.30\psi_c$ and the reduced crystal thickness $\Lambda = 0.250$, corresponding to the crystal thickness $L = 481.8$ nm, with the effects of the crystal's electrons taken into account. The area in which the yield of channeled protons is below 5 % is designated by white color, the areas in which the yields are between 5 and 10 %, 10 and 15 %, 15 and 20 %, 20 and 50 %, and 50 and 80 % by the increasing tones of gray color, respectively, and the area in which the yield is above 80 % by black color. The atomic strings defining the channel are represented by the circles lying on the x and y axes.

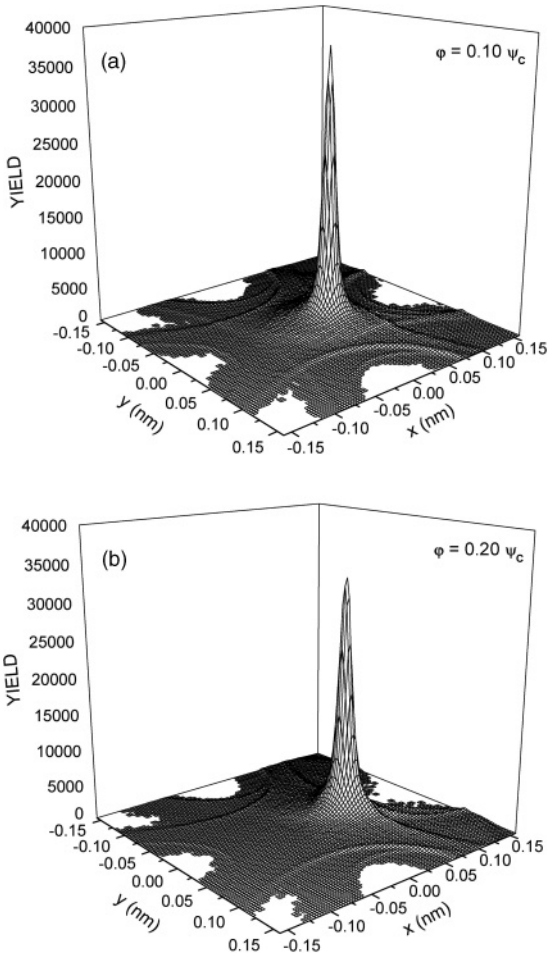

FIG. 4. The yields of channeled protons in the transverse position plane in the three-dimensional representation for the proton beam incident angles (a) $\varphi = 0.10\psi_c$ and (b) $\varphi = 0.20\psi_c$ and the reduced crystal thickness $\Lambda = 0.250$, corresponding to the crystal thickness $L = 481.8$ nm, with the effects of the crystal's electrons taken into account.

the constant proton yields are circular while the shapes of the areas of the distributions for $\varphi = \pm 0.20\psi_c$ are quasi-ellipsoidal. The widths of the distributions along the x and y axes for $\varphi = 0, \pm 0.10\psi_c$, and $\pm 0.20\psi_c$, Δx_m and Δy_m, are 15 and 15 pm, 15 and 16 pm, and 14 and 20 pm, respectively. For $\varphi = \pm 0.30\psi_c$, the distributions become broader and the shapes of their central areas representing the constant proton yields become quasirectangular. It is clear that for these values of φ, the superfocusing effect is attenuated and dissolved. Thus, as has been suggested above, the possibility to use the proton beam for probing the interior of a foreign atom inserted in the channel in the vicinity of the superfocusing point exists only for the values of modulus of φ below $\varphi = 0.20\psi_c$. Figures 4(a) and 4(b) give the spatial distributions of channeled protons in the three-dimensional representation for $\varphi = 0.10\psi_c$ and $0.20\psi_c$.

In the analysis presented in Figs. 2–4 the direction of the incident proton beam is changed along the x axis, i.e., toward the atomic strings defining the channel that intersect this axis. We have also explored the spatial distributions of channeled protons for $\Lambda = 0.250$ and the direction of the incident beam changing along line $x = y$, i.e., between the atomic strings defining the channel. The obtained results are similar to those presented in Figs. 2–4.

We have also investigated the dependencies of the yields of channeled protons around the centers of their spatial distributions on Λ in the region between 0.20 and 0.30 for $\varphi = 0.10\psi_c$ and $0.20\psi_c$ with the effects of collisions of the proton and the crystal's electrons taken into account. For the region in the transverse position plane around the center we have taken the circular region having the radius equal to $a_1 = 7.5$ pm, as in the cases of dependencies (c) and (d) shown in Fig. 1. This is in accordance with the facts demonstrated in Fig. 3 that the shapes of the areas of the distributions for $\Lambda = 0.250$ and $\varphi = 0$ and $0.10\psi_c$ representing the constant proton yields are circular while the shapes of the areas of the distributions for the same value of Λ and $\varphi = 0.20\psi_c$ are quasi-ellipsoidal. For $\varphi = 0.20\psi_c$, the circular region has approximated the quasi-ellipsoidal region. The obtained dependencies are similar to dependence (d) displayed in Fig. 1, obtained for $\varphi = 0$.

B. Rainbow patterns

Figure 5 gives the rainbow patterns in the transverse position plane for $\varphi = 0, 0.10\psi_c$, and $0.20\psi_c$ and $\Lambda = 0.250$. They were obtained without taking into account the effects of collisions of the proton and the crystal's electrons. For $\varphi = 0$, the rainbow line reduces to the rainbow point, being the superfocusing point [22]. The rainbow patterns for $\varphi = -0.10\psi_c$ and $-0.20\psi_c$ and the same value of Λ lie in the transverse position plane symmetrically with respect to the y axis to the corresponding patterns shown in the figure. The figure demonstrates that each of the rainbow patterns for $\varphi > 0$

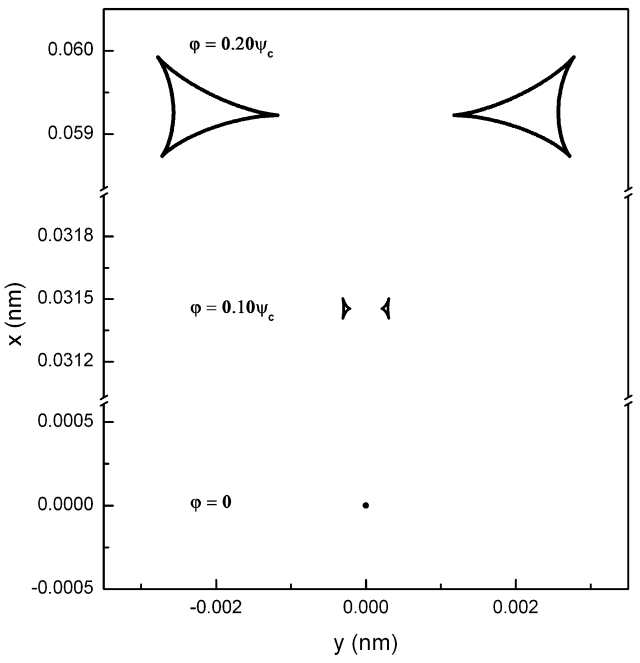

FIG. 5. The evolution of the rainbow pattern in the transverse position plane with the proton beam incident angle—for $\varphi = 0$, $0.10\psi_c$, and $0.20\psi_c$—for the reduced crystal thickness $\Lambda = 0.250$, corresponding to the crystal thickness $L = 481.8$ nm.

consists of two cusped triangular rainbow lines, each of which has two cusps directed between the atomic strings defining the channel and the third cusp directed along the y axis and toward the third cusp of the other line. The inner sides of these lines are the bright sides of the rainbows while their outer sides are the dark sides of the rainbows. As φ increases, the rainbow pattern shifts along the x axis. Also, with the increase of φ, the two rainbows become larger and more separated from each other. The comparison of these figures with Figs. 3 and 4 demonstrates that in spite of the fact that each rainbow pattern is composed of two parts, the corresponding spatial distribution of channeled protons contains only one maximum. This is explained by the fact that for each of the considered values of φ, the rainbow pattern lies within the circle of the radius as small as 2.5 pm.

Let us also analyze the evolution of the rainbow pattern in the transverse position plane with Λ around 0.250 for $\varphi = 0.10\psi_c$. The rainbow patterns for $\Lambda = 0.200$, 0.220, and 0.240 consist of a cusped rectangular line with the cusps directed between the atomic strings defining the channel. The evolution of the rainbow pattern with Λ in the region between 0.240 and 0.260 is displayed in Fig. 6. For $\Lambda = 0.245$, the rainbow pattern is composed of two cusped triangular lines, each of which with two cusps directed between the atomic strings defining the channel and the third cusp directed along the y axis and toward the third cusp of the other line. The rainbow pattern for $\Lambda = 0.250$, which is also shown in Fig. 5, consists of two cusped triangular lines, as the rainbow pattern for $\Lambda = 0.245$. The two rainbows occurring for $\Lambda = 0.250$ are separated from each other less than the two rainbows occurring for $\Lambda = 0.245$. For $\Lambda = 0.255$, the rainbow pattern contains two cusped triangular lines, each of which with two cusps directed between the atomic strings defining the channel and the third cusp directed along the y axis and away from the third cusp of the other line. These two rainbows are larger than the two rainbows occurring for $\Lambda = 0.250$ and they overlap. The rainbow pattern for $\Lambda = 0.260$ consists of a deltoidal line with two joints of its sides having the form of a swallow-tail directed along the x axis and the other two joints of its sides having the form of a cusp directed along the y axis. The rainbow patterns for $\Lambda = 0.280$ and 0.300, which are not shown in Fig. 6, contain a cusped deltoidal line with the cusps directed toward rather than between the atomic strings defining the channel. As in Fig. 5, the inner sides of all these lines are the bright sides of the rainbows while their outer sides are the dark sides of the rainbows.

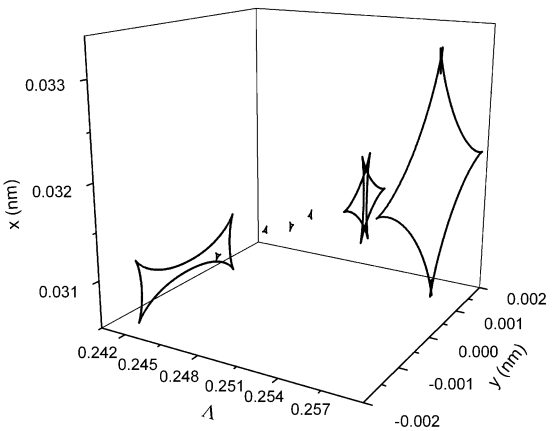

FIG. 6. The evolution of the rainbow pattern in the transverse position plane with the reduced crystal thickness in the vicinity of the superfocusing point—for $\Lambda = 0.240$, 0.245, 0.250, 0.255, and 0.260, corresponding to the crystal thicknesses $L = 462.5$, 472.2, 481.8, 491.4, and 501.1 nm, respectively—for the proton beam incident angle $\varphi = 0.10\psi_c$.

It is interesting to note that the sequences of forms presented in Ref. [22] and displayed in Figs. 5 and 6 coincide qualitatively with the unfoldings of the ${}^4X_9$ elementary catastrophe [39], which was analyzed in detail by Nye in the context of light reflection [40]. This coincidence is in agreement with our earlier finding that the ${}^4X_9$ catastrophe acts as the organizing center of crystal rainbows appearing with protons and square, rectangular, centered rectangular, and hexagonal very thin crystals with one atomic string per channel [41,42]. We think that this elementary catastrophe should be used for a simple and qualitatively accurate modeling of the changes of the rainbow pattern with φ and Λ. It should be noted here that the observed splitting of the superfocusing point induced by changing φ and Λ demonstrates the fact that a point, as a form, is not structurally stable [39].

C. Rainbow subatomic microscopy

We are now going to consider a foreign atom localized in the channel in the vicinity of the superfocusing point and exposed to the proton beam. One of the results of the proton–foreign atom interaction can be an inner-shell ionization of the atom resulting in the emission of a characteristic X-ray (PIXE) [37,38]. This is illustrated in Fig. 7. The distance between the channel walls is 271.5 pm and the radius of the foreign atom is $R_a = 100$ pm, corresponding to a sulfur atom [43]. Three beams are shown—for $\varphi = 0$, $0.10\psi_c$, and $0.20\psi_c$. Since for $\varphi = 0$, R_a is much smaller than the length of the beam neck, being $\Delta L_n = 48.2$ nm, we take that the corresponding beam diameter is constant in the interaction region and that it is equal to its diameter at the superfocusing point, being $\Delta x_m = 15$ pm. The situation is the same for $\varphi = 0.10\psi_c$ and $0.20\psi_c$. For $\varphi = 0$, the protons propagate through the foreign atom along its diameter coinciding with the z axis, and for

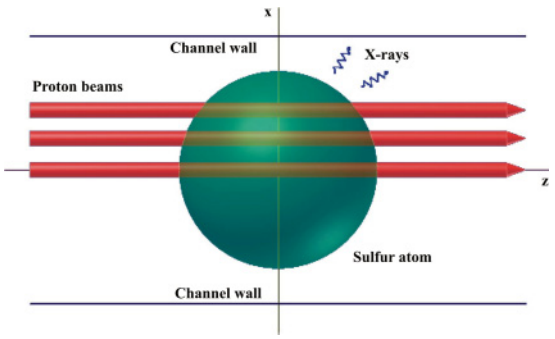

FIG. 7. (Color online) An illustration of the interactions of three proton beams—for their incident angles $\varphi = 0, 0.10\psi_c$, and $0.20\psi_c$—with the inner-shell electrons of a sulfur atom inserted in the channel at the superfocusing point resulting in the emissions of characteristic x rays (PIXE).

$\varphi = 0.10\psi_c$ and $0.20\psi_c$, they propagate through the atom along its chords being practically parallel to the z axis. The larger the value of φ, the smaller the length of the chord. This simple geometrical analysis demonstrates the possibility for measuring the differential cross-section for PIXE as a function of the proton impact parameter within the foreign atom. Thus, one could measure the electron density within the foreign atom. Such a probing of the interior of the foreign atom was named the rainbow subatomic microscopy [22].

The realization of the idea of rainbow subatomic microscopy depends crucially on the possibility to localize the foreign atom in the vicinity of the superfocusing point, i.e., to make it lie within the proton beam neck. The displacement of the foreign atom from the beam neck can be changed by varying E_0 upward or downward to move the neck forward or backward, respectively, and make the atom lie within the neck. However, the effect of thermal vibrations of the foreign atom makes its position uncertain. Since σ_{th} is comparable with the beam radius [35], one should cool the crystal to a temperature well below room temperature to make the effect less pronounced. But, even at the absolute temperature of $T = 0$ K, the quantum vibrations of the foreign atom would make the uncertainty of its position comparable with the characteristic dimension of its K shell. Using the Debey approximate treatment of the effect of thermal vibrations [29] and an estimated value of the Debey temperature of the foreign atom, being 300 K [44], one can calculate that for $T = 0$ K, the one-dimensional thermal vibration amplitude of the foreign atom is 6.2 pm. On the other hand, the characteristic dimension of the K shell of the foreign atom is 5.1 pm, and the characteristic dimensions of its L and M shells are about 25 and 100 pm, respectively [45]. This means that the effect of thermal vibrations is an obstacle for measuring the proton-induced emission of x rays from the K shell of the foreign atom, but that it does not prevent one from measuring precisely the emissions from its L and M shells.

The resolution of the microscopy is determined by the ratio of R_a and the average beam radius. In the example we consider, this ratio has the values of 13.3, 12.9, and 12.5 for the three values of φ, respectively. Thus, one can choose five values of φ, 0, $\pm 0.10\psi_c$, and $\pm 0.20\psi_c$, and obtain five well-separated measurement points. If the differential cross-section for PIXE is measured, the final result of the experiment would be the transverse projection of the electron density within the foreign atom. In this case, the sensitivity of the microscopy is determined by the way the differential cross-section depends on the electron density.

However, in order to observe experimentally the superfocusing effect, one must have an array of foreign atoms in the channels with the same transverse positions relative to the channel axes and the same longitudinal positions relative to the entrance plane of the crystal. Since the proton beam radius is considerably below R_a, the transverse positions of the foreign atoms must coincide with each other. However, the longitudinal distances of the foreign atoms from the superfocusing point do not have to coincide with each other. Instead, they must be in the region between $-\Delta L_n/2$ and $\Delta L_n/2$. One way of creating the required array of foreign atoms would be by the technique of ion implantation. The foreign atoms would be implanted in the Si crystal to form a buried single-crystalline layer with the foreign atoms at the front interface of the obtained three-layer structure facing the channels of the Si crystal [46,47]. After the implantation one would have to anneal the obtained structure to make the transverse positions of the foreign atoms within the channels at the interface coincide with each other. Such an interface would contain the required array of foreign atoms. The other way of creating the required array of foreign atoms would be by the technique of epitaxial growth. The idea is to grow on the Si crystal a single-crystalline layer with the foreign atoms at the interface of the obtained two-layer structure facing the channels of the Si crystal [16]. This would have to be followed by etching the Si crystal to adjust its thickness.

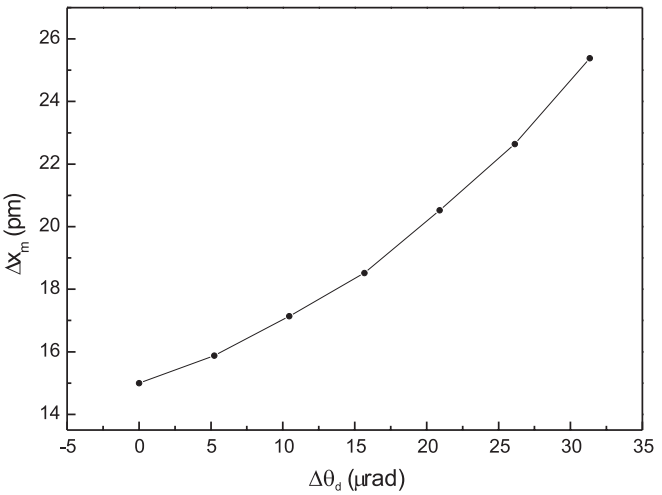

FIG. 8. The width of the spatial distribution of channeled protons along the x axis in the transverse position plane, Δx_m, as a function of the incident proton beam divergence, $\Delta\theta_d$, for the proton beam incident angle $\varphi = 0$ and the reduced crystal thickness $\Lambda = 0.250$, corresponding to the crystal thickness $L = 481.8$ nm, with the effects of the crystal's electrons taken into account.

In addition, in a superfocusing experiment one must pay special attention to the incident proton beam divergence, $\Delta\theta_d$. Figure 8 gives the dependence of Δx_m on $\Delta\theta_d$ for $\varphi = 0$ and $\Lambda = 0.250$ with the effects of collisions of the proton and the crystal's electrons taken into account. It is clear that for $\Delta\theta_d$ below about 20 μrad, Δx_m is below about 20 pm. The analysis has shown that the same is true for $\varphi = 0.10\psi_c$ and $0.20\psi_c$. Taking into account the fact, which can be seen in Fig. 2(a), that the average distance between the superfocusing maxima for $\varphi = 0$ and $0.10\psi_c$ and between the ones for $\varphi = 0.10\psi_c$ and $0.20\psi_c$ is 30.2 pm, one can conclude that for $\Delta\theta_d$ below about 20 μrad, these superfocusing maxima would be clearly separated. Such a small value of $\Delta\theta_d$ has already been attained experimentally [48]. For example, the beam collimation system consisting of two apertures of the diameters of 100 μm placed at the distance of 5 m from each other would guarantee that $\Delta\theta_d$ would be below 20 μrad.

IV. CONCLUSIONS

We have presented here a detailed study of the question how the protons in the channeling process under consideration are

distributed in space. It has been demonstrated that each of the spatial distributions of channeled protons for the proton beam incident angle φ between 0 and $\pm 0.20\psi_c$ and the reduced crystal thickness $\Lambda = 0.250$ has one strong and narrow maximum, whose displacement from the origin is below $1.3a_0$ and above $-1.3a_0$, respectively. These maxima are due to the superfocusing effect, which is explained by the dominance of the harmonic component of the continuum proton-crystal interaction potential over its anharmonic component in the region close to the channel axis. Also, we have shown that in this channeling process the rainbows occur. The rainbow patterns corresponding to the distributions for $\varphi > 0$ consist of two cusped triangular lines. For $\varphi = 0$, these two rainbow lines reduce to a point.

Besides, it has been confirmed that this channeling process can be the basis of a measurement technique with the picometer resolution, which was named the rainbow subatomic microscopy [22]. We have analyzed the process of PIXE, and demonstrated that it is possible to measure the differential cross-section for this process as a function of the proton impact parameter within the foreign atom, giving the transverse projection of the electron density within the atom.

ACKNOWLEDGMENTS

We acknowledge the support to this work provided by the Ministry of Education and Science of Serbia through project *Physics and Chemistry with Ion Beams*, No. III 45006.

[1] G. Cao, *Nanostructures and Nanomaterials: Synthesis, Properties, and Applications* (Imperial College Press, London, UK, 2004).
[2] N. Yao (ed.), *Focused Ion Beam Systems: Basics and Applications* (Cambridge University Press, Cambridge, UK, 2007).
[3] S. Bellucci, V. M. Biryukov, Y. A. Chesnokov, V. Guidi, and W. Scandale, Phys. Rev. ST Accel. Beams **6**, 033502 (2003).
[4] X. Artru, S. P. Fomin, N. F. Shulga, K. A. Ispirian, and N. K. Zhevago, Phys. Rep. **412**, 89 (2005).
[5] R. B. Alexander, G. Dearnaley, D. V. Morgan, and J. M. Poate, Phys. Lett. A **32**, 365 (1970).
[6] J. U. Andersen, O. Andreasen, J. A. Davies, and E. Uggerhøj, Radiat. Eff. **7**, 25 (1971).
[7] D. V. Vliet, Radiat. Eff. **10**, 137 (1971).
[8] M. A. Kumakhov, Radiat. Eff. **15**, 85 (1972).
[9] R. B. Alexander, P. T. Callaghan, and J. M. Poate, Phys. Rev. B **9**, 3022 (1974).
[10] F. Abel, M. B. G. Amsel, C. Cohen, and A. L'Hoir, Phys. Rev. B **12**, 4617 (1975).
[11] J. A. Ellison, Phys. Rev. B **12**, 4771 (1975).
[12] F. Abel, G. Amsel, M. Bruneaux, C. Cohen, and A. L'Hoir, Phys. Rev. B **13**, 993 (1976).
[13] J. A. Ellison and S. T. Picraux, Phys. Rev. B **18**, 1028 (1978).
[14] M. A. Kumakhov and G. Shirmer, *Atomic Collisions in Crystals* (Atomizdat, 1980, in Russian; Gordon and Breach Science Publishers, New York, USA, 1989, in English).
[15] L. C. Feldman, Crit. Rev. Solid State Mater. Sci. **10**, 143 (1981).
[16] L. C. Feldman, J. W. Mayer, and S. T. Picraux, *Materials Analysis by Ion Channeling* (Academic Press, New York, USA, 1982).
[17] G. V. Dedkov, A. M. Kumakhov, and M. Z. Sokhov, Radiat. Eff. **71**, 261 (1983).
[18] V. V. Beloshitsky, F. F. Komarov, and M. A. Kumakhov, Phys. Rep. **139**, 293 (1986).
[19] Y. N. Demkov and J. D. Meyer, Eur. Phys. J. B **42**, 361 (2004).
[20] L. Miletić, S. Petrović, and N. Nešković, Nucl. Instrum. Methods Phys. Res., Sect. B **115**, 337 (1996).
[21] L. Miletić, S. Petrović, and N. Nešković, Radiat. Eff. Def. Solids **141**, 235 (1997).
[22] N. Nešković, S. Petrović, and D. Borka, Nucl. Instrum. Methods Phys. Res., Sect. B **267**, 2616 (2009).
[23] N. Nešković, Phys. Rev. B **33**, 6030 (1986).
[24] N. Nešković and S. Petrović, J. Electron Spectrosc. **129**, 233 (2003).
[25] H. F. Krause, S. Datz, P. F. Dittner, J. Gomez del Campo, P. D. Miller, C. D. Moak, N. Nešković, and P. L. Pepmiller, Phys. Rev. B **33**, 6036 (1986).
[26] H. F. Krause, J. H. Barrett, S. Datz, P. F. Dittner, N. L. Jones, J. Gomez del Campo, and C. R. Vane, Phys. Rev. A **49**, 283 (1994).
[27] S. Petrović, L. Miletić, and N. Nešković, Phys. Rev. B **61**, 184 (2000).
[28] J. Lindhard, K. Dan. Vidensk. Selsk. Mat. Fys. Medd. **34**, No. 14, 1 (1965).
[29] D. S. Gemmell, Rev. Mod. Phys. **46**, 129 (1974).
[30] H. F. Krause and S. Datz, *Channeling of Heavy Ions through Crystalline Lattices*, Advances in Atomic, Molecular, and Optical Physics, Vol. 37 (Academic Press, New York, USA, 1996), p. 139.
[31] S. Petrović, L. Miletić, and N. Nešković, Radiat. Eff. Defects Sol. **141**, 223 (1997).
[32] S. Petrović, S. Korica, M. Kokkoris, and N. Nešković, Nucl. Instrum. Methods Phys. Res., Sect. B **193**, 152 (2002).
[33] I. V. Komarov and A. P. Shcherbakov, Vestnik Leningrad. Univ., Ser. Fiz. Khim. **16**, 24 (1979) (in Russian).
[34] Y. N. Demkov, Vestnik Leningrad. Univ., Ser. Fiz. Khim. **2**, 31 (1987) (in Russian).
[35] B. W. Batterman and D. R. Chipman, Phys. Rev. **127**, 690 (1962); Y. S. Umanskii and V. I. Prilepskii, Fiz. Tverd. Tela **7**, 2958 (1966) [Sov. Phys. Solid State **7**, 2399 (1966)].
[36] M. Abramowitz and I. A. Stegun, *Handbook of Mathematical Functions* (Dover Publications, New York, USA, 1965), p. 896.
[37] A. Denker, J. Opitz-Coutureau, J. L. Campbell, J. A. Maxwell, and T. Hopman, Nucl. Instrum. Methods Phys. Res., Sect. B **219-220**, 130 (2004).
[38] A. Denker, W. Bohne, J. L. Campbell, T. H. P. Heide, J. A. Maxwell, J. Opitz-Coutureau, J. Rauschenberg, J. Röhrich, and E. Strub, X-Ray Spectrom. **34**, 376 (2005).
[39] R. Thom, *Structural Stability and Morphogenesis* (Benjamin, Reading, USA, 1975).

[40] J. F. Nye, *Natural Focusing and Fine Structure of Light* (Institute of Physics Publishing, Bristol, UK, 1999), p. 198.
[41] N. Nešković, G. Kapetanović, S. Petrović, and B. Perović, Phys. Lett. A **179**, 343 (1993).
[42] N. Nešković, S. Petrović, G. Kapetanović, B. Perović, and W. N. Lennard, Nucl. Instrum. Methods Phys. Res., Sect. B **93**, 249 (1994).
[43] J. C. Slater, J. Chem. Phys. **41**, 3199 (1964).
[44] J. Lahtinen, P. Kantola, S. Jaatinen, K. Habermehl-Cwirzen, P. Salo, J. Vuorinen, M. Lindroos, K. Pussi, and A. P. Seitsonen, Surf. Sci. **599**, 113 (2005).
[45] C. F. Fischer, *The Hartree-Fock Method for Atoms* (Wiley, New York, USA, 1997), p. 33.
[46] R. Jebasinski, S. Mantl, C. Dieker, and W. Jäger, Nucl. Instrum. Methods Phys. Res., Sect. B **64**, 99 (1992).
[47] H. Nolte, W. Assmann, H. Huber, S. A. Karamian, and H. D. Mieskes, Nucl. Instrum. Methods Phys. Res., Sect. B **136**, 587 (1992).
[48] M. B. H. Breese, D. N. Jamieson, and P. J. C. King, *Materials Analysis Using a Nuclear Microprobe* (Wiley, New York, USA, 1996), p. 59.